# Tip-induced band bending effect and local electronic structure of Al nanoclusters on Si(111)

H. Narita, A. Kimura, and M. Taniguchi
*Graduate School of Science, Hiroshima University, 1-3-1 Kagamiyama, Higashi-Hiroshima, Hiroshima 739-8526, Japan*

M. Nakatake, T. Xie, S. Qiao, and H. Namatame
*Hiroshima Synchrotron Radiation Center, Hiroshima University, 2-313 Kagamiyama, Higashi-Hiroshima, Hiroshima 739-0046, Japan*

S. Yang, L. Zhang, and E. G. Wang
*State Key Laboratory for Surface Physics and International Center of Quantum Structure, Institute of Physics, Chinese Academy of Science, Beijing 100080, People's Republic of China*

(Received 30 May 2008; revised manuscript received 12 August 2008; published 10 September 2008)

Scanning tunneling microscopy and scanning tunneling spectroscopy (STS) have been examined for an Al nanocluster periodic array grown on *p*-type silicon substrate. Local density of states at Al and Si sites within the nanocluster has been extracted from site-resolved STS spectra by taking into account tip-induced band bending (TIBB) effect. Besides, it has been clarified that the surface-potential-energy shift caused by TIBB effect directly influences the tunneling current spectra. Consequently, a good correspondence has been found between the experimental spectra and the theoretical local density of states except for the energy gap. The energy gap has been experimentally determined as 1.7 eV, which is much larger than the predicted value. This discrepancy could be ascribed to the local-density approximation rather than the TIBB effect.

DOI: 10.1103/PhysRevB.78.115309 PACS number(s): 73.20.At, 73.22.−f

## I. INTRODUCTION

In the last two decades, several articles have been devoted to the study of fabrication of nanocluster using various metals on a large unit cell, such as Si (111) $7\times7$ reconstructed surface,[1–7] because the self-organized nanoclusters are expected to be an optimum playground in revealing quantum effects for nanotechnology such as high-density memory media, single electron transistors, and nanocatalysts.[8–10] These clusters are periodically arranged within a Si (111) $7\times7$ half unit cell (HUC) realized with the fine tuning of metal deposition and substrate temperature. Note that their surface structures are known to be different for different adsorbed atoms. Considerable effort has been made to determine atomic structures using scanning tunneling microscopy (STM) and low-energy electron diffraction (LEED) with the help of *ab initio* calculations.[1–7]

The Al nanocluster on Si (111) $7\times7$ reconstructed surface was found and its structural model was originally proposed by Yoshimura *et al.*[11] Later detailed and reasonable atomic structures were proposed by Kotlyar *et al.*,[2] and a more accurate structure was explored by Jia *et al.*[4] through the STM experiment combined with the first-principles total-energy calculation. They have shown that the Al nanocluster has six Al atoms forming a triangle, where three Si atoms are displaced from the center adatom site of $7\times7$ reconstructed surface toward the center of a HUC, as shown in Fig. 1.

Although the structural properties of Al nanocluster have been almost identified, little is known about its electronic structure. Formerly, we have performed STM/scanning tunneling spectroscopy (STS) and current imaging tunneling spectroscopy (CITS) for the Al nanocluster periodic array grown on the *n*-type Si (111) substrate,[12] where a significant energy gap of 3.3 eV was observed at 78 K. From these results, the empty-state STS spectra of Si and Al atoms within the cluster on the faulted half unit cell (FHUC) and the unfaulted half unit cell (UFHUC) have just shown a structureless feature. As is well known for metal-insulator-semiconductor (MIS) system, metal tips definitely induce a band bending on the semiconductor surface. This is called tip-induced band bending (TIBB) effect, which induces shifts of the energy position and negative differential conductivity (NDC),[13] and changes the size of energy gap[14] in the STS spectra. Resultantly, the STS spectra exhibit different features among the same semiconducting surfaces depending on density of surface states and on a degree and a polarity of carrier concentrations.

In order to obtain a unified picture of the local density of states (LDOS), we have performed STM and STS measurements of the Al nanocluster on Si (111) surface. In the present study, the TIBB effect has been carefully taken into account to extract the intrinsic LDOS.

## II. EXPERIMENT

The experiments were carried out in an ultrahigh-vacuum (UHV) chamber with a base pressure of $1.0\times10^{-10}$ mbar,

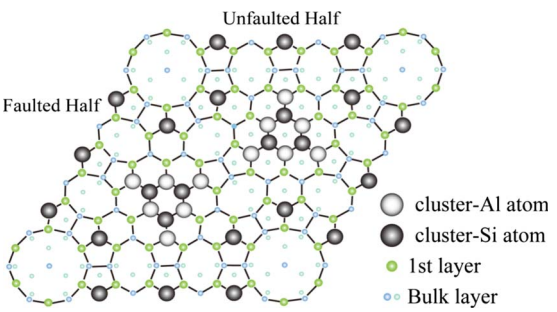


FIG. 1. (Color online) Structural model of Al nanocluster grown on Si (111) surface, as proposed by Jia *et al.* (Ref. 4).

 

using a low-temperature scanning tunneling microscope (Omicron LT-STM). We used highly *B*-doped Si (111) wafers (*p*-type), and the surface was chemically treated by a modified RCA method[15] and then immediately introduced into the UHV chamber. A clean Si (111) $7\times7$ reconstructed surface was obtained by a standard flashing procedure up to 1250 °C after outgassing at about 500 °C for several hours. Subsequently, Al atoms were carefully deposited using a well-outgassed homemade evaporator with an AlN crucible showing a high thermal conductivity. All of the STM images and STS spectra were obtained at 78 K using the same STM tip made of chemically etched tungsten wire. The STS spectrum was taken by averaging ten spectra of each atomic site on the same HUCs. The periodic array of Al nanocluster has been prepared by about 0.24 monolayer (ML)-Al deposition (1 ML$=7.8\times10^{14}$ atoms/cm$^2$). During the STS measurement, in order not to be affected by barrier resonances[16] as well as a peak shift depending on current set point,[17] the sample bias $V_S$ and the tunneling current $I_t$ was kept from −4.0 to +4.0 V, and below 0.3 nA, respectively. For the STS spectrum, the normalized conductance $(dI/dV)/(I/V)$ could be adopted. Since a divergence of intensity due to a negligible tunneling current in the energy-gap region would be expected, a normalized tunneling conductance is modified here with a corrected $I/V$ denoted as $\overline{I/V}=\sqrt{(I/V)^2+0.02^2}$, which was originally introduced by Prietsch *et al.*[18]

## III. RESULTS AND DISCUSSION

Figures 2(a) and 2(b) show the filled and empty-state STM images of well-ordered Al nanocluster arrays observed at 78 K. It is found that the STM images at positive ($V_S=+2.5$ V) and negative ($V_S=-2.5$ V) sample biases show many different features. The filled-state STM image clearly shows Al nanoclusters forming a honeycomb periodic array on the $7\times7$ surface. In contrast, six protrusions can be identified within the nanocluster as recognized in the empty-state STM image. Note that the empty-state STM image tells us that the Al nanocluster can be classified into four types of clusters, as shown in Fig. 2(c). It is recognized that Si atoms occupying the corner adatom sites are, in some cases, replaced by Al atoms, which are easily identified as bright spots surrounding the nanoclusters, as formerly discussed by Kotlyar *et al.*[2] As the number of Al atoms increases, the HUC containing three extra bright spots dominates the surface. The maximum number of substituted Al atoms per HUC is three. Thus the cluster with three replaced Al atoms at the corner Si adatom sites of a HUC is named as "*n*3." In this way, one can find the other clusters called "*n*0," "*n*1," and "*n*2" depending on the number of replaced Al atoms. We basically need to discuss STS spectra of all the clusters but the electronic structure deduced from the LDA calculation and our STS spectra did not change irrespective of the number of Al atoms (not shown). Consequently, we will focus on the electronic structure of *n*0 cluster, which would provide us with a fundamental knowledge of LDOS. To obtain the LDOS in atomic scale, we have probed three atomic sites (cluster Si, corner Al, and edge Al) on FHUC and UFHUC.

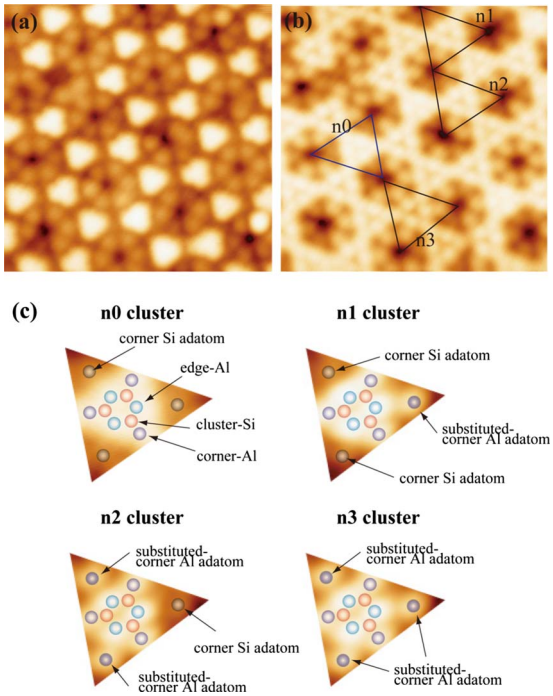


FIG. 2. (Color online) (a) Filled state ($V_S=-2.5$ V) and (b) empty-state ($V_S=+2.5$ V) STM images of well-ordered Al nanocluster array observed at 78 K ($10\times10$ nm$^2$), which are acquired simultaneously. (c) Empty state ($V_S=+2.5$ V) STM image of four different Al nanoclusters with different number (0–3) of replaced Al atoms at the corner Si adatom site, as denoted by $n0-n3$.

Thick solid lines in Fig. 3 show the site-resolved STS spectra of cluster-Si atom as well as of corner- and edge-Al atoms. Here, we note that these STS spectra have been obtained for the same sample surface. All the STS spectra of the Al nanocluster show a distinct energy gap of 1.8 eV and each spectrum shows several peak structures at the positive sample bias, whereas the filled-state STS spectra are rather broadened except for the cluster-Si site. In contrast, for edge-

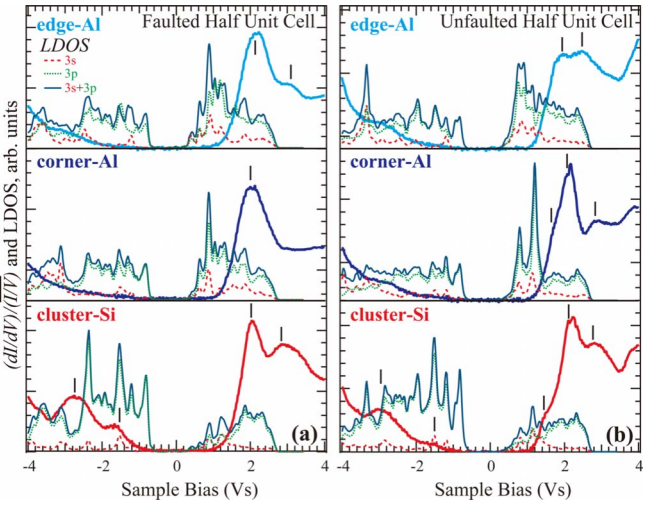


FIG. 3. (Color online) Site-resolved STS spectra (thick line) and theoretical LDOS (thin line) of (a) FHUC and (b) UFHUC for edge-Al, corner-Al, and cluster-Si sites.

TABLE I. Peak positions (in electron volts) in the site-resolved STS spectra taken from the results in Fig. 3.

| Atomic site | FHUC | UFHUC |
|---|---|---|
| edge Al | +2.14, +3.11 | +1.92, +2.47 |
| corner Al | +2.00 | +1.70, +2.10, +2.81 |
| cluster Si | −2.73, −1.56, +2.04, +2.82 | −2.99, −1.50, +2.10, +2.78 |

and corner-Al sites on both HUCs, the STS spectra in the negative bias region show very weak and broad features. In the positive bias region, clear peak structures are found, and their peak positions and spectral shapes are different among various atomic sites. The STS spectra of edge-Al site show two peaks. The first peak of the edge-Al site appears at $V_S=+2.14(+1.92)$ V and the second peak is found at $V_S=+3.11(+2.47)$ V for FHUC (UFHUC). The energy positions of these peaks are higher for FHUC than those for UFHUC. For the UFHUC of the corner-Al site, the sharp peak is found near +2.0 V followed by the higher energy satellite and the weak shoulder is found just below the intensity maximum. In contrast, only a single peak is found for the FHUC at the positive sample bias. It was noticed that the spectral features are much different between FHUC and UFHUC for both of the edge- and corner-Al sites. The STS spectra of the cluster-Si site mainly show two peaks in the positive $V_S$ region. Their energy positions are a little different between two HUCs, as shown in Table I. However the spectra of cluster-Si sites show broad but recognizable peak structures even in the negative $V_S$ region, as shown in the bottom of Fig. 3. The shoulder structure is also recognized just below the first peak only for UFHUC, which is similarly observed in the corner-Al site. The spectral weight of both Al sites is significantly suppressed in the negative sample bias region where only a weak feature is recognizable around $V_S=-2.8$ V.

Next, the observed STS spectra will be compared with theoretical LDOS.[19] Thin lines in Fig. 3 show the theoretical LDOS of edge-Al, corner-Al, and cluster-Si sites for FHUC and UFHUC, respectively. Here, the Si 3*s* and 3*p* orbitals, and Al 3*s* and 3*p* orbitals are taken into account, whose binding energies are located in the limited region of −4.0–+2.9 eV relative to the Fermi energy ($E_F$). Partial LDOS of 3*s* and 3*p* orbitals are also denoted with dashed and dotted lines, respectively. The calculated LDOS clearly shows an insulating energy gap of about 0.6 eV. Overall, the calculated LDOS of two Al sites dominates in the empty state, whereas those of cluster-Si sites show a larger weight in the filled state. Moreover, the calculated bandwidth in the unoccupied state is about 2.5 eV, where the maximum band edge is located at +2.7 eV regardless of atomic sites.

In more detail, the LDOS of the edge-Al site in FHUC shows a sharp peak structure around +1.0 eV in the empty state but rather weak structures are found in the filled state. The feature of the calculated LDOS for UFHUC seems to be similar to that of FHUC but the Al 3*p* derived states are located at lower energy than that of FHUC. In contrast, the marked difference between FHUC and UFHUC is noticeable for the corner-Al site. A distinct doublet structure appears at +0.79 and +1.20 eV in the UFHUC, while the peak at higher energy is suppressed for FHUC where a lower energy peak remains with a small shift to higher energy. As seen in the edge-Al site, the LDOS in the filled state is also smaller than that in the empty state. Contrary to these Al sites, the LDOS of cluster-Si site dominates in the occupied state as stated above. For FHUC, the distinct structures are found at −0.83, −1.54, and −2.36 eV. It is noticed that the calculated sharp peak at −2.4 eV in FHUC is much suppressed in UFHUC.

Experimental STS spectra show an energy onset at +1.0 eV for all of the atomic sites in the unoccupied state. There also appears a dip around +3.5 eV. As a result, the observed energy bandwidth can be estimated as +2.5 eV in the unoccupied state, which agrees well with the calculated LDOS. For the FHUC of the edge Al, the observed sharp peak structure is well reproduced in the theoretical LDOS with higher energy shift by ~1 eV. The enhanced weight in the higher energy region relative to the first peak above $E_F$ for UFHUC can be reasonably explained by the relatively higher weight in the corresponding energy range of the theoretical LDOS. The difference in the experimental LDOS of the corner-Al site between two different HUCs is likewise explained by the calculation. The presence of low-energy shoulder in UFHUC may be ascribed to the sharp peak just above the energy gap in the theoretical LDOS because the experimentally determined energy difference between shoulder and peak of ~0.4 eV fits well with the calculated value. Besides, the absence of the shoulder structure in FHUC is also consistent with the calculation. As in the case of the edge-Al site, the observed sharp peaks above $E_F$ is shifted to higher energy by ~0.9 eV compared to the calculated LDOS. In the occupied state of the cluster-Si site, the experimental LDOS is enhanced, which is simply understood as the larger DOS with several distinct peak structures compared to those for the Al sites. The characteristic peaks at −1.5 and −2.8 eV in the experiment can be reasonably found in the calculation if the energy difference of 0.5–1.0 eV is taken into account. It has been experimentally observed that the Si *sp* bands dominate the occupied states whereas the Al *sp* bands mainly contribute to the unoccupied states. The observed trend is in good agreement with the calculated LDOS, meaning that there could be charge transfer from Al to Si sites. Moreover, the calculation shows an edge at −2.8 eV, which might correspond to the common dip at −3.4 eV in the experimental STS spectra of the Al and Si sites for both HUCs. In this way, the overall agreement between the experimental STS spectra and the theoretical LDOS has been obtained in terms of the relative energy positions and spectral shapes. It is noted that our former STS results for the same Al nanocluster phase on the *n*-type Si (111) substrate are consistent with the present experimental results with the *p*-type Si substrate in the occupied state.[12] However, the corresponding STS spectra with the *n*-type Si surface have shown the onset at ~+2.2 V, which is higher by about 1 V compared to the case of the *p*-type substrate. Besides, the observed sharp peaks in the unoccupied state for the *p*-type surface have been smeared out for the *n*-type surface. The marked difference in the unoccupied state clearly indicates that the experimental feature of STS spectra

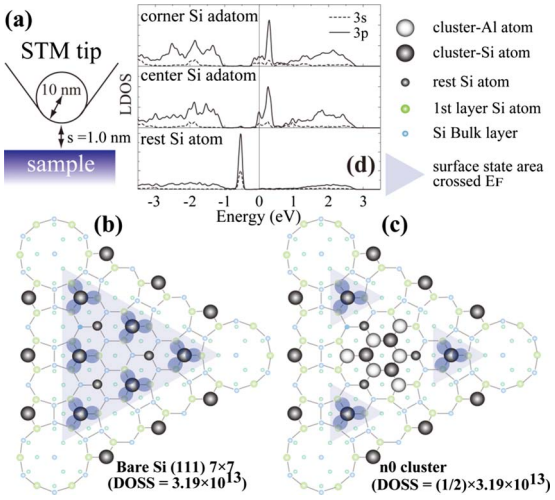


FIG. 4. (Color online) (a) STM tip configuration assumed for the parameter in the TIBB calculation. [(b) and (c)] Schematics of DOSS of bare Si (111) $7\times7$ surface and $n0$ cluster on the UFHUC, respectively. (d) Calculated LDOS of corner Si, center Si, and rest Si adatoms on $7\times7$ surface.

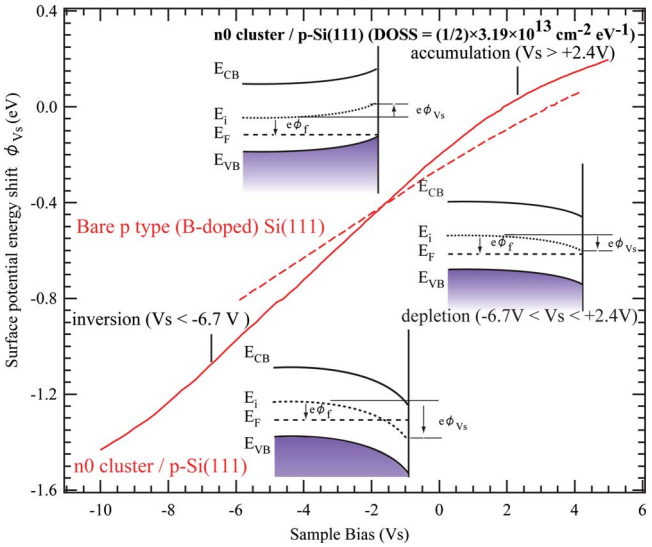


FIG. 5. (Color online) Calculated surface-potential-energy shift $\phi_{V_S}$ as a function of sample bias ($V_S$). Solid and broken lines show the curve of $n0$ cluster on $p$-type silicon substrate as well as of bare $p$-type silicon substrate. The inset figures show the energy diagrams in the accumulation, depletion, and inversion regimes near vacuum-semiconductor interface.

strongly depends on the carrier dopant of the substrate.

To solve the discrepancy for the different empty-state STS spectra of the Al nanocluster between the $p$-type and $n$-type silicon substrates, we have tried to reveal the surface-potential shift resulting from the TIBB effect, showing the carrier dynamics as described by the typical STM theory. Weimer *et al.*[20] suggested that the electric field between the STM metal tip and the semiconductor sample induces a band bending at the semiconductor surface due to a weak electron screening. This physical picture is often expressed by using the simple rigid-band structure. As a result, one can extract the intrinsic LDOS from the present normalized conductance and the calculated results also help us to understand carrier dynamics underneath the probing point. In our study, we have adopted the calculation method proposed by Feenstra.[21]

The setting parameters used for $B$-doped $p$-type (Sb-doped $n$-type) silicon substrate are as follows:[21–24] a band gap of 1.12 eV for Si, a doping density of $6\times10^{18}(5\times10^{19})$ cm$^{-3}$, an acceptor (donor) level of 0.045 (0.039) eV, a dielectric constant of 11.9, a sample temperature of 78 K, a charge neutrality level (CNL) of 0.4 eV, a sample electron affinity of $\chi$=4.05 eV, and a tip work function $\phi_m$=4.55 eV. Other parameters of tip configuration for computation are tip-sample separation, and tip radius of 1.0 and 10 nm, respectively [Fig. 4(a)]. The tip configuration in this work is actually unknown but is considered to be insensitive to the potential-energy shift of the calculated result on the sample surface.[17] Therefore, typical parameters are chosen here. It should be noted that the density of surface states (DOSS) (cm$^{-2}$ V$^{-1}$) that crosses the Fermi level plays an important role[25] because electrons in the surface state near $E_F$ mainly contribute to the screening from the electrostatic potential energy and significantly change the electric-field gradient near the nonmetallic surface. The DOSS is estimated by the actual value from the STM images, such as the edge distance of $7\times7$ HUC ($d$=2.7 nm), and there is one surface state per HUC above three corner Si adatoms and three center Si adatoms, as shown in Fig. 4(b). As is evident from the theoretical site-resolved LDOS shown in Fig. 4(d), no surface state that is related to the TIBB effect is provided from the rest Si atom. Therefore, two surface states per unit cell of Si (111) $7\times7$ can contribute to the TIBB effect, corresponding to the value of DOSS, $3.19\times10^{13}$ cm$^{-2}$ V$^{-1}$. In the $n0$-type Al nanocluster, it can be assumed that the DOSS decreases by half due to disappearance of the surface states at $E_F$ because three dangling bonds of center Si adatoms are hybridized with Al $sp$ states, as shown in Fig. 3. This supposition is also clearly explained from the results of the LDA calculation at each atomic site as shown in Fig. 3. In the realistic case, the other types of $n1-n3$ clusters are also distributed over the Al nanocluster surface. Surface states at $E_F$ decreases from two to zero for $n1-n3$ clusters. However, our DOSS estimation for the realistic case shows that surface-potential-energy shift $\phi_{V_S}$ only varies in the range of 0.1 V near $V_S$=+2.1 V.

Figure 5 shows the calculated results of surface-potential-energy shift $\phi_{V_S}$ for the bare $p$-type Si (111) $7\times7$ surface and the $n0$ cluster on the $p$-type Si (111) surface as a function of the sample bias. The surface-potential-energy shift of the bare $p$-type Si (111) changes from −0.63 to +0.05 V in the bias range of −4.0–+4.0 V, as denoted with broken line in Fig. 5. Here, we find that the depletion appears in the present bias range. In the same way, the $n0$ cluster on the $p$-type Si (111) has two regimes, such as the accumulation ($V_S>+2.4$ V) and the depletion ($-6.7$ V$<V_S<+2.4$ V). By comparing the curves of the bare Si (111) with that of the $n0$ cluster, the slope for the $n0$ cluster is larger than that for the bare Si (111). From these results, it is reasonably understood that the normalized conductance spectra of the $p$-type Si (111) surface show clear peak structures near $V_S$=+2.0 V because it is located in the regime of accumu-

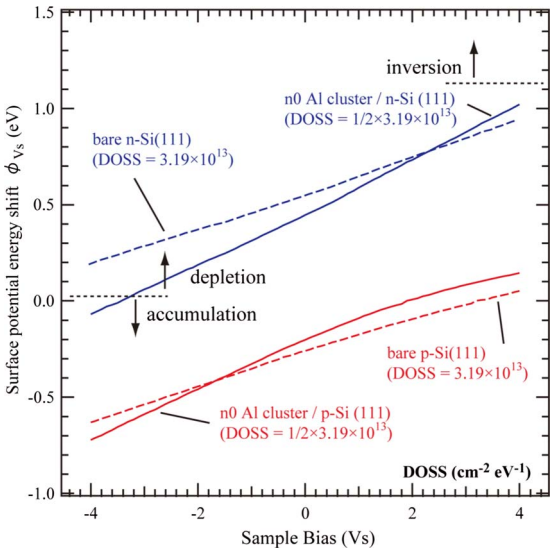


FIG. 6. (Color online) Calculated surface-potential-energy shift $\phi_{V_S}$ as a function of sample bias ($V_S$). Solid and broken lines show the curves of $n0$ cluster on the Si (111) and the bare Si (111), respectively.

lation, as shown in Fig. 5, in contrast to the case of the $n$-type substrate.

Figure 6 shows the calculated results of the surface-potential-energy shift $\phi_{V_S}$ as a function of sample bias for the $n$-type and $p$-type Si surfaces. Looking at the curves of the bare $n$-type Si (111) and the $n0$ cluster on the $n$-type Si (111), the surface carrier of the $n0$ cluster shows three different regimes of accumulation ($V_S < -3.3$ V), depletion ($-3.3$ V $< V_S < +4.5$ V), and inversion ($V_S > +4.5$ V). This means that the carrier concentration gradually decreases with increasing sample bias from $-3.3$ to $+4.5$ V just below the probing point. Therefore, the carrier concentration takes minimum around $V_S = +4.0$ V, and then, actually, the STS spectra of the $n0$ cluster on the $n$-type Si (111) substrate have shown a significant gap of 3.3 V and a structureless feature due to an insufficient current flow from tip to substrate.[12] From the present result, it is important to know the carrier behavior in the probing area for STM/STS on the insulating surface. At least, if one carries out STM/STS experiment to observe fundamental local electronic structure using the insulating surface formed on Si (111) $7 \times 7$, a $p$-type substrate would be preferable.

Now we try to reconsider the LDOS of Al nanocluster on the $p$-type silicon substrate with an inclusion of TIBB effect. Table II lists the peak positions of each atomic site after taking into account TIBB effect, which have been corrected with the formula binding energy (BE) ($=V_S - \phi_{V_S}$). In this analysis, we have calculated the energy shift, assuming that several factors concerned in the surface-potential-energy shift are independent of the atomic species and surface atomic arrangement. According to these results, the experimental energy gap of the Al nanocluster ($n0$ cluster) at 78 K is reevaluated from 1.8 to 1.7 eV. However, this result is still much larger than the predicted energy gap of 0.6 eV.[19] We have also tried to calculate the surface-potential-energy shift with different CNLs in the range of 0–0.6 eV by TIBB calculation program but only a slight change of $\pm 0.10$ eV has been obtained for the energy gap. It is known that the LDA based calculation underestimates the energy gap of semiconductors, as typically found in bulk Si and Ge. The LDA predicts a nearly zero energy gap for Ge (Ref. 26) and a small energy gap of 0.45 eV for Si, which is 0.72 eV smaller than the experimental value of 1.17 eV.[27] In analogy to these cases, the predicted smaller energy gap can be ascribed to the LDA itself.

TABLE II. Corrected energy positions (in electron volts) of site-resolved STS spectra after taking into account the TIBB effect.

| Atomic site | FHUC | UFHUC |
|---|---|---|
| edge Al | +2.12, +3.02 | +1.92, +2.43 |
| corner Al | +1.99 | +1.69, +2.07, +2.74 |
| cluster Si | −2.18, −1.16, +2.03, +2.75 | −2.40, −1.13, +2.09, +2.71 |

## IV. CONCLUSIONS

We have investigated the local electronic structure of the Al nanocluster fabricated on the $p$-type Si (111) $7 \times 7$ surface from STS spectra, which has been compared with the calculated LDOS with consideration of the TIBB effect. The site-resolved STS spectra have shown several distinct structures at each atomic site, which are consistent with the theoretical LDOS in terms of relative energy positions and their shapes. It turned out that the TIBB derives the different features of STS spectra with different carrier concentrations of substrates. The energy gap of the Al nanocluster phase has been determined as 1.7 eV. The experimental energy gap larger than the predicted value has been ascribed mainly to the limitation of LDA.

## ACKNOWLEDGMENTS

The authors acknowledge R. M. Feenstra for his support of TIBB calculation. This work was partly supported by a Grant-in-Aid for Scientific Research from the Ministry of Education, Culture, Sports, Science, and Technology of Japan (Contract No. 17340112), and one of the authors (H.N.) was also supported by Iketani Science and Technology Foundation (Contract No. 0171067-A).

[1] J. L. Li, J. F. Jia, X. J. Liang, X. Liu, J. Z. Wang, Q. K. Xue, Z. Q. Li, J. S. Tse, Z. Zhang, and S. B. Zhang, Phys. Rev. Lett. **88**, 066101 (2002).
[2] V. G. Kotlyar, A. V. Zotov, A. A. Saranin, T. V. Kasyanova, M. A. Cherevik, I. V. Pisarenko, and V. G. Lifshits, Phys. Rev. B **66**, 165401 (2002).
[3] M. Y. Lai and Y. L. Wang, Phys. Rev. B **64**, 241404(R) (2001).
[4] J. F. Jia, X. Liu, J. Z. Wang, J. L. Li, X. S. Wang, Q. K. Xue, Z. Q. Li, Z. Zhang, and S. B. Zhang, Phys. Rev. B **66**, 165412 (2002).
[5] H. H. Chang, M. Y. Lai, J. H. Wei, C. M. Wei, and Y. L. Wang, Phys. Rev. Lett. **92**, 066103 (2004).
[6] K. Wu, Y. Fujikawa, T. Nagao, Y. Hasegawa, K. S. Nakayama, Q. K. Xue, E. G. Wang, T. Briere, V. Kumar, Y. Kawazoe, S. B. Zhang, and T. Sakurai, Phys. Rev. Lett. **91**, 126101 (2003).
[7] S. C. Li, J. F. Jia, R. F. Dou, Q. K. Xue, I. G. Batyrev, and S. B. Zhang, Phys. Rev. Lett. **93**, 116103 (2004).
[8] K. Bromann, C. Felix, H. Brune, W. Harbich, R. Monot, J. Buttet, and K. Kern, Science **274**, 956 (1996).
[9] H. Brune, M. Giovannini, K. Bromann, and K. Kern, Nature (London) **394**, 451 (1998).
[10] S. Sun, C. B. Murray, D. Waller, L. Folks, and A. Moser, Science **287**, 1989 (2000).
[11] M. Yoshimura, K. Takaoka, and T. Tao, J. Vac. Sci. Technol. B **12**, 2434 (1994).
[12] H. Narita, M. Nakatake, M. Kakeya, A. Kimura, T. Xie, S. Qiao, H. Namatame, and M. Taniguchi, e-J. Surf. Sci. Nanotechnol. **4**, 208 (2006).
[13] S. Loth, M. Wenderoth, L. Winking, R. G. Ulbrich, S. Malzer, and G. H. Döhler, Phys. Rev. Lett. **96**, 066403 (2006).
[14] R. M. Feenstra and Joseph A. Stroscio, J. Vac. Sci. Technol. B **5**, 923 (1987).
[15] W. Kem and D. A. Puotinen, RCA Rev. **31**, 187 (1970).
[16] R. S. Becker, J. A. Golovchenko, D. R. Hamann, and B. S. Swartzentruber, Phys. Rev. Lett. **55**, 2032 (1985).
[17] R. M. Feenstra, G. Meyer, and K. H. Rieder, Phys. Rev. B **69**, 081309(R) (2004).
[18] M. Prietsch, A. Samsavar, and R. Ludeke, Phys. Rev. B **43**, 11850 (1991).
[19] L. Zhang, S. B. Zhang, Q. K. Xue, J. F. Jia, and E. G. Wang, Phys. Rev. B **72**, 033315 (2005).
[20] M. Weimer, J. Kramar, and J. D. Baldeschwieler, Phys. Rev. B **39**, 5572 (1989).
[21] R. M. Feenstra, J. Vac. Sci. Technol. B **21**, 2080 (2003).
[22] The doping density of each wafer is within the range specified by supplier.
[23] S. M. Sze, *Physics of Semiconductor Device* (Wiley, New York, 1981), p. 21.
[24] J. Tersoff, Phys. Rev. Lett. **52**, 465 (1984).
[25] R. M. Feenstra, S. Gaan, G. Meyer, and K. H. Rieder, Phys. Rev. B **71**, 125316 (2005).
[26] C. Kittel, *Introduction to Solid State Physics* (Wiley, New York, 2005).
[27] G. B. Bachelet and N. E. Christensen, Phys. Rev. B **31**, 879 (1985).